

GAS DYNAMICS IN THE GALACTIC BAR REGION FROM N-BODY AND SPH SIMULATIONS

R. FUX

*Geneva Observatory,
Ch. des Maillettes 51, CH-1290 Sauverny, Switzerland*

Abstract. Self-consistent hybrid N -body and SPH simulations are used to give a new and coherent interpretation of the main features standing out from the HI and CO longitude-velocity observations within the Galactic bar. In particular, the traces of the gas associated to the Milky Way's dustlanes can be reliably identified and the 3-kpc arm appears as a gaseous stream rather than a density wave. The bar and the gaseous nuclear ring in the simulations undergo synchronised and long lived oscillations around the centre of mass, and the gas flow always remains non-stationary, suggesting a transient nature of the observed gas kinematics.

1. Introduction

During the last decade, there has been accumulating evidence that the Milky Way is a barred galaxy (e.g. Gerhard 1999 for a recent review), confirming the early presumption of de Vaucouleurs (1964) based on the observed gas kinematics. In particular, the HI and CO longitude-velocity ($\ell - V$) distributions betray large non-circular motions near the Galactic centre which have been attributed to gas moving on non self-intersecting closed x_1 orbits of the barred Galactic potential. The direct detection of the bar has motivated several recent gas dynamical studies (e.g. Wada et al. 1994; Englmaier & Gerhard 1999; Weiner & Sellwood 1999).

Fux (1999) has tried to give a new and coherent interpretation of the so far poorly understood dominant features seen in the gaseous $\ell - V$ diagrams within the bar region (see Figure 1), based on high resolution N -body and SPH simulations and on observed properties in external barred galaxies. The present contribution gives a brief summary of the main results and some complements.

2. Simulations

The stellar and gas dynamics is modelled in a self-consistent way by the N -body and SPH techniques, starting from plausible bar unstable axisymmetric initial conditions. The simulations are divided into two parts. First we run only the collisionless stellar and dark components



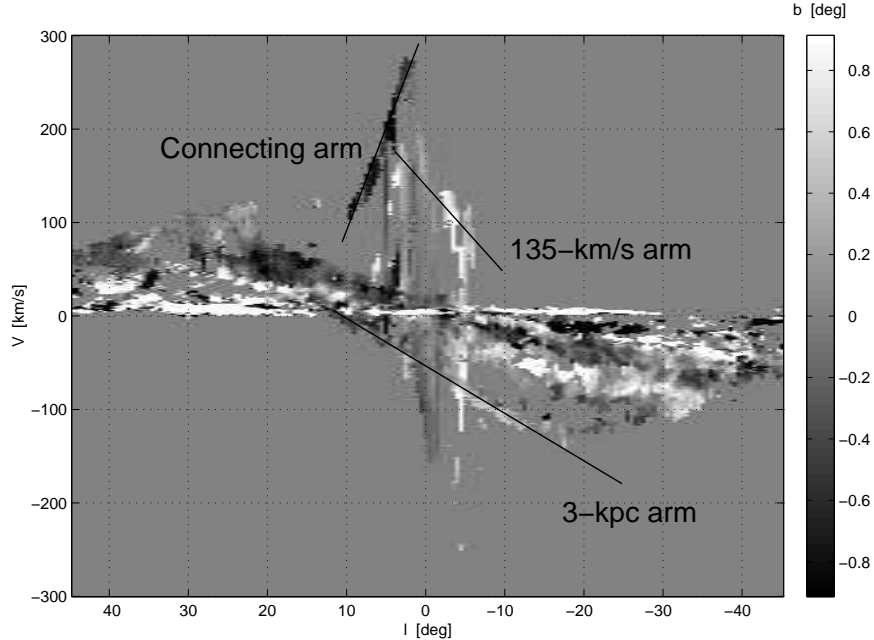


Figure 1. Emission weighted mean latitude of ^{12}CO in the $\ell - V$ plane. Dark and white indicate respectively gas below ($b < 0$) and above ($b > 0$) the Galactic plane. The data are from Dame et al. 1987.

for 5 Gyr, keeping the gas fixed (simulation lxx), and then the gas is softly released at two different times, $t = 1800$ and 2400 Myr, with a sound speed $c_s = 10 \text{ km s}^{-1}$ (simulations l10 and l10' respectively). The total number of particles is $\sim 4 \times 10^6$, with 150 000 gas particles, and the simulations are evolved without imposed symmetries. Some animations of simulation l10, including live $\ell - V$ diagrams, are available at <http://obswww.unige.ch/~fux>.

The stellar bar forms at around $t = 1.2$ Gyr, well before releasing the gas, and its pattern speed naturally adjusts to real physical constraints. Its projected surface mass density gives a good representation of the dereddened COBE/DIRBE K-band map for realistic viewing points relative to the bar. One of the most relevant dynamical properties of the bar is its offcentring on Gyr timescales with respect to the centre of mass of the global mass distribution (see Figure 9 in Fux 1999). The displacement can reach several 100 pc and the revolution frequency of the density centre amounts to $20 - 30 \text{ km s}^{-1} \text{ kpc}^{-1}$.

The gas flow in the simulations, which take into account the gas self-gravity and the gravitational interaction of the gas with the stellar arms, is non-stationary and affected by substantial asymmetries. Beside the nuclear ring, discussed in the next section, the gaseous structures

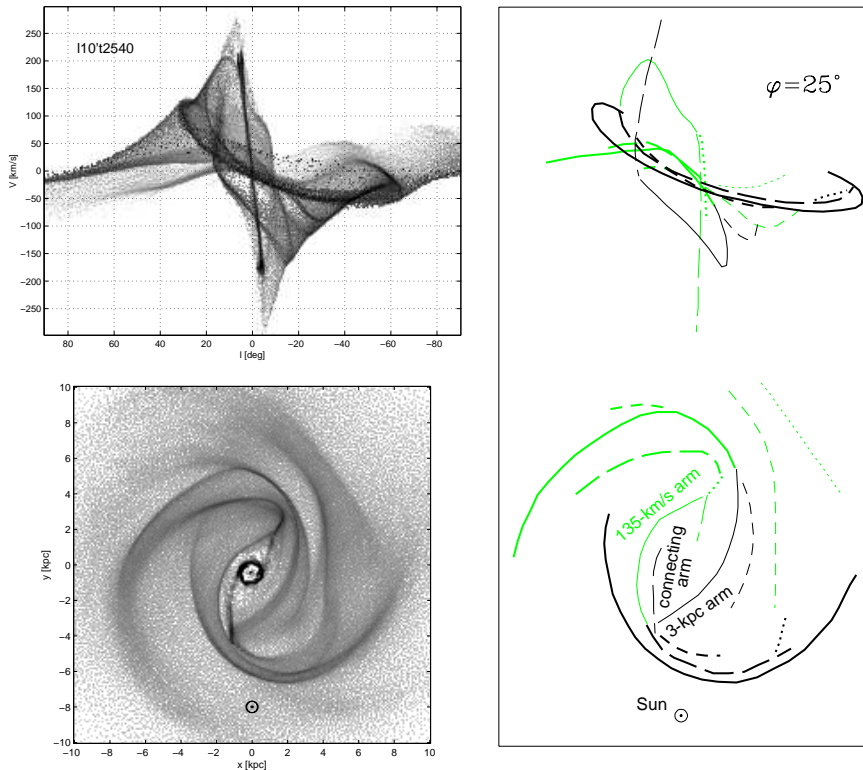


Figure 2. Model 110't2540, selected as one of the models reproducing best most of the observed features in the region $|\ell| \lesssim 35^\circ$. *Top left:* ℓ - V diagram based on the gaseous particles within $|b| < 2^\circ$. *Bottom left:* face-on projection of the gas distribution, with the location of the observer indicated by the \odot symbol. The bar inclination angle is 25° and the corotation radius 0.55 relative to the Sun's galactocentric distance. *Right:* link between the spiral arms and their ℓ - V traces.

in the bar region may be classified according to two types (see frame $t = 2066$ Myr in Figure 4 for an ideal case):

- The *axis shocks*, which connect the ends of the bar to the nuclear ring and are characterised by very strong velocity gradients.
- The *lateral arms*, which roughly join the bar ends avoiding the nuclear ring by a large bow.

At specific times and for a location of the observer such that the corotation radius of the bar is 4.0–4.5 kpc and the bar inclination angle $\varphi \sim 25^\circ$, the simulations reveal models which compare fairly well with observations (see Figure 2 for one of our favorite models). These models allow an original interpretation of the main HI and CO ℓ - V features in terms of axis shocks and lateral arms, which is further developed in Sections 4 and 5.

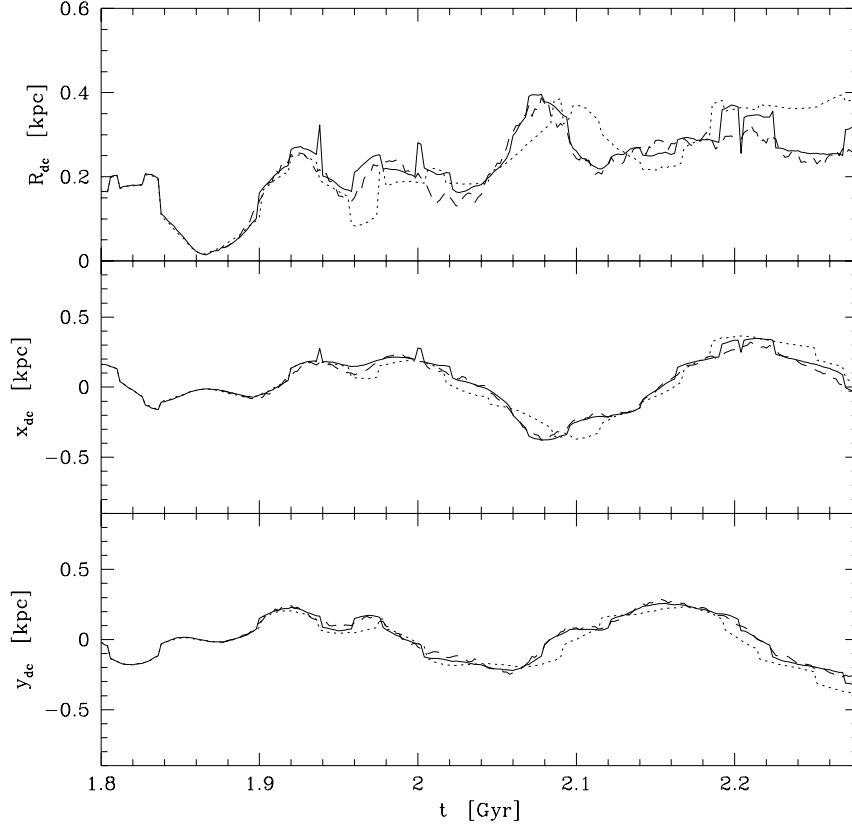


Figure 3. Radial, x - and y -displacements of the stellar density centre (solid lines) and of the gaseous nuclear ring (dashed lines) in the live gas simulation l10. The dotted lines indicate the displacement of the stellar density centre in the fixed gas simulation lxx.

3. Nuclear ring/disc

The mass distribution in our simulations involves a single inner Lindblad resonance, at $R_{\text{ILR}} = 1.7$ kpc and 1.6 kpc from the mass density centre in the scaled models l10t2066 and l10t2540 respectively. This is the radius below which the anti-bar x_2 orbits exists and a nuclear ring of such orbits rapidly concentrates at $R \lesssim R_{\text{ILR}}/2$. The nuclear ring produces a marked dip in the $\Omega - \kappa/2$ curve, but which never reaches a value below the bar pattern speed Ω_{P} , as expected for the ring to be stable. The size of the ring is set by the geometry of the axis shocks: the energy dissipation when the gas of these shocks hits the ring prevents the nuclear ring to extend beyond the central offset of the shocks. One shortcoming of our models is that the nuclear ring lies beyond the dense

nuclear molecular gas observed within 1.5° from the Galactic centre, corresponding to $R \lesssim 200$ pc.

The nuclear ring closely follows the density centre displacement of the stellar bar, apparently without a significant time delay (Figure 3). The cause of the offcentring is not very clear but it is certainly not induced by the gas component alone, because the bar leaves the centre of mass before the gas has been released. Moreover, a comparison between the live (l10) and fixed (lxx) gas simulations reveals only small differences in the trajectory of the stellar density centres, despite the fact that the bar rotates faster in the former case.

4. Connecting arm

The connecting arm (Figure 1) has not been given much attention since the direct detections of the Galactic bar by Blitz & Spergel (1991) and others. A remarkable success of our simulations is that some snapshots can reproduce very precisely this $\ell - V$ feature (see Figure 2 and $t = 2066$ Myr in Figure 4).

The connecting arm obviously corresponds to an axis shock. Most high resolution hydro simulations in rotating barred potentials display such shocks (e.g. Athanassoula 1992) and they are believed to be related to the prominent dustlanes observed in many early-type external barred galaxies. These dustlanes indeed seem to coincide with gaslanes and velocity field measurements reveal velocity changes of order 200 km s^{-1} across them (Reynaud & Downes 1998; Laine et al. 1999). Thus, according to our models, the connecting arm is the gaseous trace of the near-side branch of the Milky Way's dustlanes. The far-side branch is seen in Figure 1 as a vertical feature near $\ell = -4^\circ$. The same figure also reveals that the near-side branch of these dustlanes lies below ($b < 0$) the Galactic plane and the far-side branch above it.

Velocity elongated features like the one at $\ell \approx 5.5^\circ$ could be gas lumps which are just about to cross the near-side dustlane, undergoing the strong velocity gradient of the associated shock.

5. 3-kpc arm

The 3-kpc and the 135-km s^{-1} arms are lateral arms, with the former arm ending in the near-side axis shock. They are the inner prolongations of spiral arms in the disc and their velocity asymmetry at $\ell = 0$ comes from the fact that the 135-km s^{-1} arm passes much closer and faster to the Galactic centre.

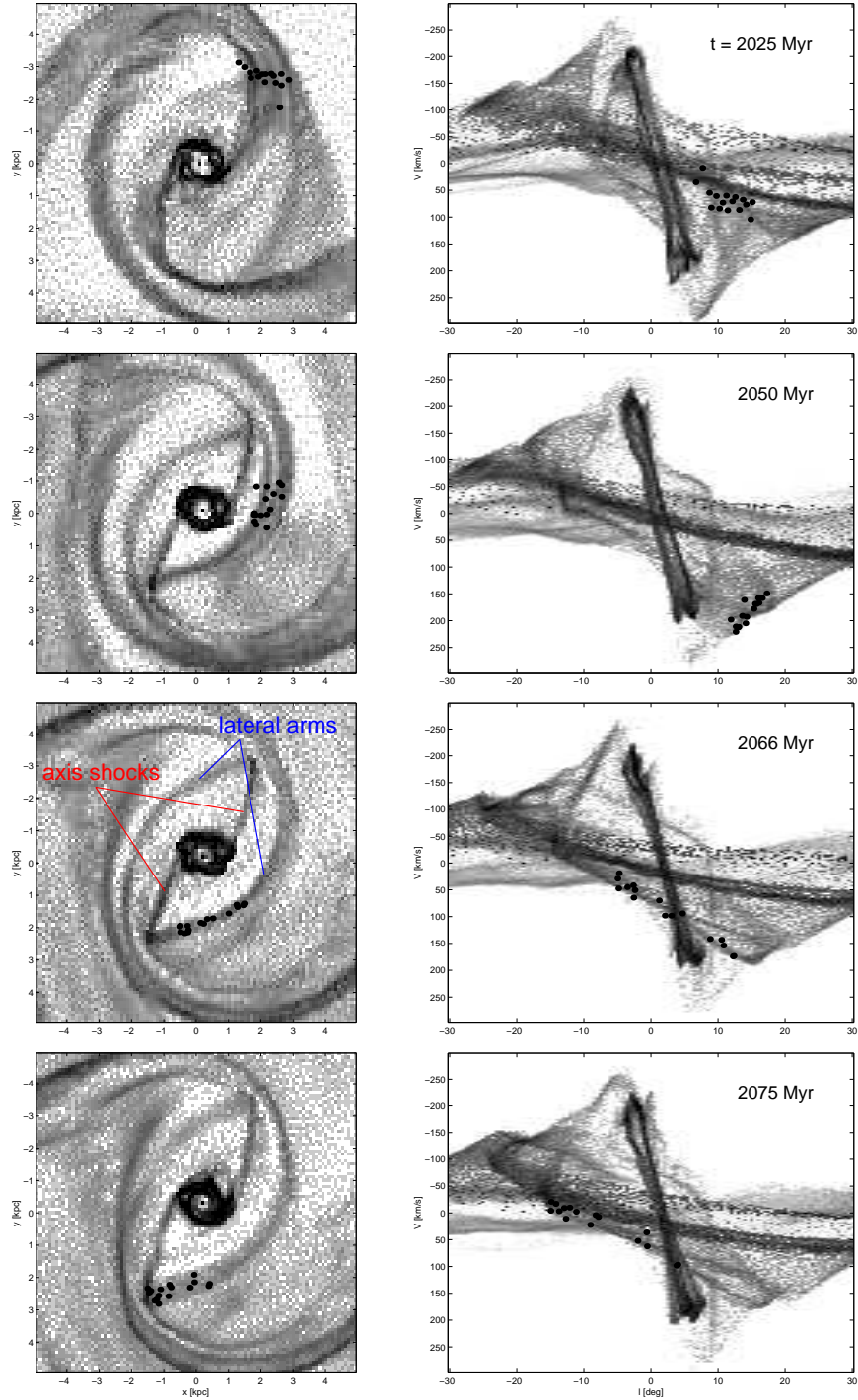


Figure 4. See next page.

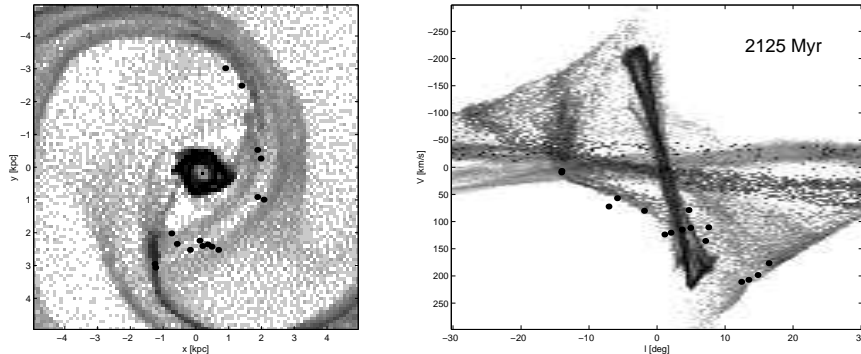


Figure 4. Continued. In simulation 110, trajectories of collisionless particles with phase space coordinates similar to the 3-kpc arm gas at $t = 2066$ Myr, i.e. located within 100 pc and 14 km s^{-1} of the gas particles in this arm having spatial densities over $0.1 M_{\odot} \text{ pc}^{-3}$. The $x - y$ plots are in the rotating frame of the bar and the $l - V$ plots for a comoving observer such that the bar inclination angle remains at 25° . In the frames at $t = 2125$ Myr, the bar has been rotated by π . The collisionless particles always remain confined inside the 3-kpc arm as they pass from one end of the bar to the other, illustrating that the gas in this arm follows ballistic orbits with only little dissipation and that the matter keeps locked in the arm.

Sevenster (1997) has outlined 9 OH/IR stars following very closely the 3-kpc arm pattern. From their outflow velocities and assuming disc metallicities, she infers masses between 3.5 and $6 M_{\odot}$ and thus ages between 100 and 350 Myr for these stars, corresponding to a few galactic rotations. Since these stars are still coincident with a gaseous density maximum, Sevenster (1999) concludes that the 3-kpc arm cannot be a density wave, but rather is part of an inner ring as observed in many external barred galaxies (Buta 1996).

In our simulations, the lateral arms cannot be considered as true density waves. Indeed, in the rotating frame of the bar, gas on the lateral arms moves in a direction almost parallel to the maximum density line of the arms and thus there is no net propagation of them relative to the sustaining medium. Consequently, comoving stars may be captured inside such an arm longer than if the flow were perpendicular to the arm. Figure 4 shows the trajectories of collisionless particles whose phase space coordinates are similar to the gaseous “3-kpc” arm in model 110t2066. At $t = 2025$ Myr, these particles are all concentrated at the far end of the bar, where they are almost corotating with the bar. Referring to the enhanced star formation rate observed at the bar ends of several external galaxies (e.g. Reynaud & Downes 1998 for NGC 1530), which may result from the compression of the gas as lateral arms strike the outer part of the axis shocks, this concentration may suggest that the OH/IR stars tracing the 3-kpc arm have formed in this region. If this

is correct, then these OH/IR stars should be ~ 40 Myr old and thus more massive than $6 M_{\odot}$ (in the simulations, the particles tracing the 3-kpc arm turn round the bar in $2\pi/(\Omega - \Omega_P) \approx 120$ Myr). It is also possible that these OH/IR stars formed earlier at the near end of the bar, made more than half a rotation round the bar on quasi-periodic x_1 orbits and finally mixed with the 3-kpc arm before passing again through their place of birth (see $t = 2125$ Myr in Figure 4). In this case, the age of the OH/IR stars would be ~ 100 Myr, becoming consistent with Sevenster's (1997) estimation. In principle, this interpretation can even be generalised to several pre-rotations of the stars before they are observed within the 3-kpc arm, though phase mixing will spread the stars around the bar.

Acknowledgements

The author thanks L. Martinet, D. Pfenniger, D. Friedli, L. Blitz, F. Combes, P. Englmaier, O. Gerhard and J. Sellwood for suggestive discussions, and D. Pfenniger, D. Friedli and W. Benz for the original version of the N -body/SPH code.

References

- Athanassoula E. 1992, *MNRAS* **259**, 345
 Blitz L., Spiegel D.N. 1991, *ApJ* **379**, 631
 Buta R. 1996. In: Buta R., Crocker D.A., Elmegreen B.G. (eds.) Proc. IAU Coll. 157, ASP Conf. Series 91, *Barred Galaxies*. ASP, San Francisco, p. 11
 Dame T.M., Ungerechts H., Cohen R.S. et al. 1987, *ApJ* **322**, 706
 de Vaucouleurs G. 1964. In: Kerr F.J., Rodgers A.W. (eds.) Proc. IAU-URSI Symp. 20, *The Galaxy and the Magellanic Clouds*. Australian Acad. of Sci., Canberra, p. 88
 Englmaier P., Gerhard O. 1999, *MNRAS* **304**, 512
 Fux R. 1999, *A&A* **345**, 787
 Gerhard O.E. 1999. In: Merritt D.R., Valluri M., Sellwood J.A. (eds.) *Galaxy Dynamics*. ASP Conf. Series (in press, astro-ph/9902247)
 Laine S., Kenney J.D.P., Yun M.S., Gottesman S.T. 1999, *ApJ* **511**, 709
 Reynaud D., Downes D. 1998, *A&A* **337**, 671
 Sevenster M.N. 1997, PhD thesis. Leiden University, Amsterdam
 Sevenster M.N. 1999, submitted to *MNRAS*
 Wada K., Taniguchi Y., Habe A., Hasegawa T. 1994, *ApJ* **437**, L123
 Weiner B.J., Sellwood J.A. 1999, submitted to *ApJ* (astro-ph/9904130)